Novel Gain of Function Mouse Model of KCNT1-Related Epilepsy

Sarah L. Olguin[1,2], Daniel Davis[3,4]; Ammara Rehman[1,5], Sean W. Berg[1,2], Elizabeth Sahagun[1,2]; Payton S. Oswalt[3], Mandar Patil[1,5], Paula D.M. Sullivan[1,5], Bing Zhang[6], **Elizabeth C. Bryda[3,4*], Roy Ben-Shalom[1,5*], Jill L. Silverman[1,2*]**

Affiliations:
[1]MIND Institute, University of California Davis School of Medicine, Sacramento, CA 95817, USA. [2]Department of Psychiatry and Behavioral Sciences, University of California Davis School of Medicine, Sacramento, CA 95817, USA. [3]Veterinary Pathobiology, College of Veterinary Medicine, University of Missouri, Columbia, MO, 65201, USA. [4] MU Animal Modeling Core University of Missouri, Columbia, MO, 65201, USA. [5]Department of Neurology, University of California Davis School of Medicine, Sacramento, CA 95817, USA [6]Division of Biological Sciences, University of Missouri, Columbia, MO 65201, USA.

***Co-Corresponding Authors:**
Jill L. Silverman
MIND Institute and Department of Psychiatry and Behavioral Sciences
4625 2nd Ave Suite 1001A
Sacramento, CA 95817
Phone: 916-734-8531
jsilverman@ucdavis.edu

***Co-Corresponding Authors:**
Elizabeth Bryda, Ph.D.
Department of Veterinary Pathobiology, University of Missouri
4011 Discovery Drive
Columbia, MO 65201
Phone: (573) 882-5504
brydae@missouri.edu

***Co-Corresponding Authors:**
Roy Ben-Shalom
MIND Institute and Department of Neurology
rbenshalom@ucdavis.edu

Keywords: *KCNT1, Epilepsy, epileptic encephalopathy, behavior, seizures, excitability, mouse model, hyperexcitability, epilepsy, channel, potassium, DEE*

Conflict of Interest: The authors declare no conflicts of interest.
Acknowledgements: This work was supported by the MIND Institute's Intellectual and Developmental Disabilities Resource Center NIH P50HD103526 (LA), the NIMH ARTP R01MH117130 (JAG), and Research Council Grant URC-21-027 from the Office of Research,

University of Missouri (ECB). The mouse model was generated by the University of Missouri Animal Modeling Core.

Funding Sources: This work was supported by the MIND Institute's Intellectual and Developmental Disabilities Resource Center P50HD103526 and an MDBR award from the KCNT1 Foundation and the University of Pennsylvania Orphan Disease Center (JLS, SLO), Hartwell Foundation Biomedical Fellowship (JLS; SLO), and Research Council Grant URC-21-027 from the Office of Research, University of Missouri (ECB).

54 **Abstract**

55 *KCNT1*-related epilepsy is an autosomal dominant neurodevelopmental disorder with at
56 least 64 known human variants, each with unique electrophysiological and epileptic
57 characteristics. A multi-disciplinary collaboration generated a novel mouse model (C57BL/6-
58 *Kcnt1*^{em1Bryd}) carrying the G269S variant, corresponding to human G288S, located within the
59 coding region of the channel pore. Network excitability of cultured cortical neurons from
60 *Kcnt1*$^{+/G269S}$ exhibited sustained hyperexcitability and hypersynchronous bursting while
61 *Kcnt1*$^{G269S/G269S}$ neurons showed early excessive bursting followed by network collapse,
62 suggesting excitotoxicity. *Kcnt1*$^{+/G269S}$ displayed poor motor coordination, erratic breathing, and
63 increased apneas. Critically, *Kcnt1*$^{+/G269S}$ were more susceptible to thermal-induced seizures in
64 early life. In summary, these data: (i) provide a novel mouse model of KCNT1-related epilepsy,
65 (ii) provide strong *in vitro* evidence of neuronal hyperexcitability, (iii) illustrate early-life seizures
66 as a functional outcome measure, and (iv) lay the groundwork for future analysis of neural activity
67 *in vivo* and modeling circuit level dynamics *in vitro* and *in silico*.

68

69 **Significance Statement**

70 Gain-of-function mutations in the sodium-gated potassium channel KCNT1 have been
71 linked to pediatric epilepsy of varying severity. The human *KCNT1* variant G288S (G269S in
72 mice) is linked to Autosomal Dominant Nocturnal Frontal Lobe Epilepsy (ADNFLE), Epilepsy
73 of Infancy with Migrating Focal Seizures (EIMFS), and other severe developmental epileptic
74 encephalopathies. There are currently no therapeutics to prevent the progression of *KCNT1*-
75 related epilepsy, therefore, the scientific community requires a novel mouse model that is well
76 characterized, *in vitro* and *in vivo,* to screen and assess targeted therapeutics. Herein, we
77 engineered a novel mouse to assess developmental and adult phenotypes resulting from the
78 G288S/G269S variant, *in vitro* and *in vivo*, to advance translation toward therapeutic testing for
79 individuals with *KCNT1*-related epilepsy.

Introduction

Genetic studies have shown that approximately one-third of neurodevelopmental disorders (NDDs) are associated with gene mutations affecting neuronal ion channels, emphasizing their critical role in brain pathology[1-3]. To understand how these mutations alter channel kinetics, *in vivo* experimental models are essential[4-7]. The *KCNT1* gene encodes a sodium activated potassium (K_{Na^+}) channel that regulates neuronal excitability by influencing the resting membrane potential and hyperpolarization following action potentials. Mutations in *KCNT1* result in diverse electrophysiological profiles, contributing to distinct epileptic syndromes such as Epilepsy of Infancy with Migrating Focal Seizures (EIMFS), Autosomal Dominant Nocturnal Frontal Lobe Epilepsy (ADNFLE), West syndrome, and Ohtahara syndrome[8]. To date, 64 *KCNT1* mutations have been identified, across 248 individuals[9,10], however, few *in vivo* mouse models exist, which has curbed therapeutic development.

Homozygous *Kcnt1*$^{-/-}$ mice exhibit poor motor ability and impaired motor learning, however, seizure related metrics were similar to wild-type (WT) control mice[11]. A mouse model carrying the R455H variant (human R474H) resulted in increased potassium currents in glutamatergic neurons and suppression of inhibitory neuron firing[12,13]. This occurs when dysfunctional channels activate rapidly in response to sodium influx during action potential upstroke, which can limit sodium channel inactivation and promote hyperexcitability. Video-EEG of *Kcnt1*$^{+/R455H}$ mice revealed persistent interictal spikes, spontaneous seizures, and a reduced threshold for pentylenetetrazol (PTZ)-induced seizures[11].

The homozygous P924L variant causes frequent debilitating seizures and developmental compromise[14]. Another experimental model, Y777H (human Y796H) exhibited sleep disturbances due to elevated seizure bouts and length[15]. Both *Kcnt1*$^{+/Y777H}$ and *Kcnt1*$^{Y777H/Y777H}$

103 were susceptible to kainic acid (KA) and PTZ-induced seizures (Shore et al., 2020). Conditional
104 expression of Y777H had no effect on glutamatergic neurons but, increased subthreshold K_{Na^+}
105 currents in inhibitory neurons[16]. This cell type-specific modulation creates network imbalance,
106 functionally silencing certain inhibitory neurons while excitatory transmission remains intact or
107 enhanced[10].

108 Finally, the loss-of-function (LOF) variant, P932I, is associated with severe early infantile
109 epileptic encephalopathy (EE) and abnormal myelination[17]. Each *KCNT1* variant affects channel
110 kinetics differently—altering activation thresholds, open probability, and current amplitude[10].
111 These differences impact neuronal excitability and seizure susceptibility, varying considerably
112 across variants, neuronal subtypes, and background strain of the rodent model[18-20] adding
113 complexity to understanding circuit-level dysfunction in *KCNT1*-related epilepsies.

114 D*rosophila melanogaster* lack a *KCNT1* ortholog, allowing for the introduction of the
115 human *KCNT1* (*hKCNT1)* gene. While the WT *hKCNT1* gene showed no phenotype, expression
116 of GOF human variants exhibited seizure activity rates of 41% (G288S), 48% (R398Q), and 38%
117 (R928C), respectively[21,22]. Zhang's laboratory illustrates that *hKCNT1* G288S and R928C
118 mutations increased potassium conductance, impaired larval locomotion, hyperpolarized the
119 resting membrane potential, and reduced muscle resistance[21,22]. Consistent with these findings,
120 expression of the G288S variant in HEK cells exhibits: (i) a 21-fold increase in K_{Na^+} current
121 amplitude; (ii) an approximate 20% increase in channel open probability; (iii) a hyperpolarizing
122 shift in activation threshold, reducing voltage sensitivity; and (iv) minimal changes in channel
123 kinetics[10]. These data encouraged the generation of the *Kcnt1* GOF G288S (G269S in mice)
124 experimental model, termed B6-*Kcnt1*^{em1Bryd}. This model enabled targeted characterization of

125 electrophysiological properties *in vitro* and functional outcomes *in vivo* which provide a valuable
126 platform for studying *KCNT1*-related epilepsy.

127 **Materials and Methods.**

128 ***Generation of the G288S Variant (G269S Mouse Model):*** All experimental procedures were
129 performed in accordance with the National Institutes of Health (NIH) Guide for the Care and Use
130 of Laboratory Animals and approved by the Institutional Animal Care and Use Committees
131 (IACUC) at the University of Missouri and University of California, Davis School of Medicine.
132 The novel *Kcnt1* mutant mouse model was generated by the MU Animal Modeling Core
133 (Columbia, MO) using a standard knock in method involving CRISPR/Cas9 genome editing. The
134 strategy for generating the *Kcnt1* exon 11 codon change was to replace the wild-type mouse *Kcnt1*
135 gene codon GGG with AGC creating a missense mutation. Glycine (G) is replaced by serine (S)
136 at amino acid position 269 in the mouse *Kcnt1* protein which mimics the G288S human variant.
137 C57BL/6J (stock #000664) animals were purchased from the Jackson Laboratory (Bar Harbor,
138 ME). Super ovulated females (4-5 weeks of age) were mated to stud males (~10 weeks of age)
139 overnight and zygotes were collected the following morning. sgRNAs were ordered as chemically
140 modified synthetic sgRNAs through Synthego (Redwood City, CA). The chemical modifications
141 on each sgRNA were 2′-O-methyl analogs and 3′ phosphonothioate internucleotide linkages at the
142 first three 5′ and 3′ terminal RNA residues. The repair template was chemically synthesized by
143 IDT (Coralville, IA) as a 200bp single-stranded DNA oligo (ssODN). The ssODN was
144 complementary to the non-target strand and contained symmetrical homology arms. An additional
145 silent mutation was introduced for genotyping purposes.

146 ***sgRNA sequence:*** 5′-TCCAGGTGCTGGATCCCAC-3′. Repair template sequence (sgRNA
147 sequence disrupted by desired mutation): 5′-

148 CTGCTGCAGCCTCTCCCCCACTGCTGCAGCCCCAGCCCCACTGCTGCAGCCCCAGCC
149 CCACTGCTGCAGCCCTGATCTTCCTGTTTCTAGGACCTGT**A**G**C**ATCCAGCACCTGGA
150 GCGAGCAGGTGGCAACTTGAACCTGCTGACCTCCTTCTACTTCTGCATCGTGACTTTC
151 TCAACTGTGGGCTTCGGTGATGTGAC -3′. A mix containing a final concentration of 3.0μM
152 sgRNA, 2.0μM enhanced specificity Cas9 protein (Sigma) and 1.6μM ssODN was made
153 immediately prior to electroporation. CRISPR sgRNA/Cas9 RNP complexes were formed by
154 gently mixing the sgRNA and Cas9 protein together and incubating at room temperature for 10min.
155 After RNP formation, the ssODN repair template was added to the mixture. Using a NepaGene21
156 electroporator along with a 1.5-mm gap glass slide electrode, zygotes were electroporated under
157 the following conditions: Poring pulse: 40V, 3.5ms length, 50ms interval, 10% decay rate, positive
158 polarity (x4 pulses) Transfer pulse: 5V, 50ms length, 50ms interval, 40% decay rate, alternating
159 polarity (x5 pulses). Manipulated zygotes were then surgically transferred to pseudo-pregnant
160 surrogate CD1 females (8 weeks of age) purchased from Charles River Laboratories (Wilmington,
161 MA). Multiple animals carrying the desired single base pair change were identified by genotype
162 analysis and confirmed by nucleotide sequence analysis of the region around the base pair change.
163 The founders confirmed to carry the mutation were backcrossed to C57BL6/J for 2 generations
164 and then to C57BL6/NJ (Jackson laboratory #005304) for 2 generations to establish the strain
165 C57BL/6NJ *Kcnt1*^{em1Bryd} which is available at the Mutant Mouse Resource and Research Center
166 at the university of Missouri (MMRRC#075727) and is available upon request at www.nmrrc.org.
167 In spring 2021, animals were transferred to UC Davis, School of Medicine (Sacramento, CA) to
168 establish a colony. This colony was maintained by backcrossing to C57BL/6J for >10 generations.
169 ***Genotyping:*** Genomic DNA was extracted by placing a small amount of tissue (ear or tail) in
170 100μl alkaline lysis reagent (25mM NaOH and 0. mM EDTA at a pH of 12) and heating at 95 ˚C

171 for 1hr. This was followed by addition of 100µl neutralization buffer (40mM Tris-HCl) with
172 vortexing for 5secs to mix. The PCR primers were Kcnt1.F1: 5'-cattccacactgcagccctgtctct-3'and
173 Kcnt1.R1: 5'-caagggtgacacagatcaggatgaccac- 3'. The 25µl reaction contained the following:
174 12.5µl EmeraldAmp® Supermix (Takara Bio USA Inc., San Jose, CA); 10.0µl H_2O; 0.75µl
175 Forward primer (10µM); 0.75µl Reverse primer (10µM); 1µl genomic DNA (~5-50ng). Thermal
176 cycler conditions were 1) 95 °C, 3mins, 2) 95 °C, 30secs, 3) 69 °C, 30secs, 4) 72 °C, 1min. Steps
177 2-4 were repeated 40 times, 5) 72°C, 7mins, 6) 4 °C, hold. The expected PCR amplicon = 403 bp.
178 Following PCR amplification, 2.8µl CutSmart buffer and 1.0µl *BtsC*I (20 units) (New England
179 Biolabs, Ipswich, MA) were added directly to the PCR reaction and incubated at 50°C for 2hrs.
180 Gel electrophoresis was performed with a 3% agarose gel in 1X TAE buffer at 80V for 1hr.
181 Expected restriction fragment sizes: wild type allele = 19bp, 23bp, 42bp, and 319bp; mutant allele
182 = 19bp, 23bp, 42bp, 113bp, 206bp. The 319bp fragment in the wild type allele is cut into 113bp
183 and 206bp fragments in the mutant allele.
184 ***Cell Culture:*** Test mice were generated by crossing male and female *Kcnt1*$^{+/G269S}$ to yield pups of
185 three genotypes (*Kcnt1*$^{+/+}$, *Kcnt1*$^{+/G269S}$, and *Kcnt1*$^{G269S/G269S}$) and neonatal cortices (PND 0-2) were
186 collected. Primary cortical neuron-glia cultures were prepared as previously described[23,24]. Briefly,
187 cortices were minced with a razor blade prior to incubation in Hibernate A containing papain and
188 DNase. The tissue was then triturated with glass pipettes to dissociate cells from the extracellular
189 matrix (Bellco Glass, Vineland, NJ). Dissociated cells were counted and plated as described below.
190 ***High Density Microelectrode Array Plating:*** MaxWell Biosystems high density microelectrode
191 arrays (HD-MEAs) were used to assess electrophysiological activity of primary neuronal cultures,
192 as previously described[25,26]. MaxTwo 6-well HD-MEA plates were sterilized, filled with 2mL of
193 plating medium (Neurobasal Plus medium (Gibco, ThermoFisher Scientific), 2% B27 Plus

194 supplement (×50) (Gibco, ThermoFisher Scientific), 1x GlutaMAX supplement (Invitrogen), 10%
195 heat-inactivated horse serum (Invitrogen), and HEPES buffer (1M, pH 7.5) (Fisher Scientific)),
196 then incubated for 2 days at 37°C with 5% CO_2. On the day of cell plating, the plating media was
197 removed, and chips washed with sterile water, coated with primary coating (50µl of 0.07%
198 polyethyleneimine (PEI, Sigma-Aldrich)), and incubated for 1hr. The primary coating was
199 removed, the chips were washed 3 times with sterile water, and vacuum dried. Secary coating (50ul
200 Laminin (0.02 mg/mL; Sigma-Aldrich)) was applied and incubated (~ 1hr) until ready to plate
201 cells. The laminin coating was removed, 50uL of primary cortical cells were added to the HD-
202 MEAs, yielding approximately 125,000 cells per chip, and incubated for 1hr before the addition
203 of 2mL plating medium. 24 hours later, 50% of media was removed and replaced with cell culture
204 maintenance media (Dulbecco's Modified Eagle Medium (DMEM) supplemented with GlutaMax,
205 D-glucose and sodium pyruvate (Gibco, ThermoFisher Scientific) and 10% horse serum). Media
206 changes occurred twice weekly by removing 50% of the media and replacing it with an equal
207 volume of cell culture media. Neural activity was recorded twice a week as described below.
208 ***HD-MEA Electrophysiological Recordings and Data Processing:*** HD-MEA recordings were
209 performed between days *in vitro* (DIV) 3 to 30 to capture the developmental trajectories of
210 dissociated neuronal cultures. Due to differences in recording schedules across experiments, some
211 DIVs varied slightly between litters (e.g., DIV 13 vs 14, DIV 27 vs. 28). Each session began with
212 the Activity Scan Assay, which recorded 30-sec segments across the entire chip under 'Sparse 7x'
213 configuration to assess overall activity of the chip. Based on spike amplitude and spatial
214 distribution, 1,020 electrodes were selected from regions exhibiting high activity (spike amplitude)
215 to maximize neuron coverage in the Network Scan Assay. Spontaneous activity was recorded for
216 300s at a 10 kHz sampling rate using the MaxTwo device (MaxWell Biosystems).

217 Data processing focused on two aspects: (1) The activity of the culture over time, and (2)
218 network-level dynamics reflecting population synchrony and communication. Raw extracellular
219 signals were bandpass filtered between 300Hz and 3,000Hz to isolate multi-unit activity (MUA).
220 Spike detection was performed using a threshold set at five times the standard deviation of baseline
221 noise. A recording channel was considered active if it exceeded a predefined minimum firing rate
222 and spike amplitude threshold. The mean firing rate and mean spike amplitude were computed
223 from all active channels to assess the overall culture health and neuronal proliferation. To
224 characterize network-level activity, detected spikes were transformed into spike raster plots and
225 binned to generate population firing rates. A Gaussian kernel was applied to these binned spike
226 trains to estimate a continuous measure of population activity, capturing burst dynamics and
227 synchronous events. Statistical comparisons between genotypes were conducted using repeated
228 measures ANOVA over time and one-way ANOVAs followed by tukey's post hoc tests for
229 selected group comparisons. To ensure analytical consistency, adjacent DIVs with ±1 day variation
230 were grouped during analysis. All analyses were conducted using custom MATLAB R2024 scripts
231 in combination with the MaxWell Biosystems Toolbox (v23.2).

232 ***Subjects for Developmental Milestones, Behavioral Assays, and Seizure Susceptibility:*** All mice
233 were housed in a temperature- and humidity-controlled vivarium maintained on a 12:12 light-dark
234 cycle and tested during the light cycle. Animals were fed a standard diet of Teklad global 18%
235 protein rodent diets 2918 (Envigo, Hayward, CA, USA). Wild-type (WT) and heterozygous
236 *Kcnt1*$^{+/G269S}$ offspring were labeled by paw tattoo over postnatal days (PND) 2-4 using non-toxic
237 animal tattoo ink (Ketchum Manufacturing Inc., Brockville, ON, Canada). Tail biopsies (1–2 mm)
238 from pups were taken for genotyping, following the UC Davis IACUC policy regarding tissue
239 collection. Mice were weaned at PND21, and group housed by sex with 2-4 animals per cage.

240 Assays were performed in order of least to most stressful and between the hours of 9:00 AM PST
241 and 4:00 PM PST during the light phase. All behavior testing was conducted by an experimenter
242 blinded to genotype and included both sexes. Mice were allowed to habituate in their home cages
243 in a dimly lit room adjacent to the testing room for 1hr prior to the start of testing to limit any
244 effect of transporting between the vivarium and testing suite. Between subjects, testing apparatus
245 surfaces were cleaned using 70% ethanol and allowed to dry.

246 ***Behavioral Assays:*** Four Cohorts of mice were used for a combination of developmental
247 milestones, seizure-related outcomes, behavioral phenotypes, and respiratory physiology, with full
248 details below. Cohort 1 was used to assess developmental milestones (PND 3, 5, 9, and 11,
249 **Supplemental Table 1**) with behavioral testing order: open field, rotarod, novel object
250 recognition, contextual and cued fear conditioning and, a two hit seizure assessment using low
251 stimulus electroconvulsive threshold (ECT, Ugo Basile, Gemonio (VA), Italy) and high dose
252 (lethal) chemoconvulsant seizure induction with pentylenetetrazol (PTZ) intraperitoneally (i.p.).
253 These were not counterbalanced for order of administration because the PTZ dose is lethal,
254 therefore it had to be the "sec hit." To assess epileptogenesis or epileptic progression, while
255 simultaneously characterizing changes in seizure susceptibility with respect to prior epileptic
256 events, animals were initially exposed to an electroconvulsive induced seizure to eliminate
257 duration and severity variability at lower chemo convulsant doses[27]. Cohort 2 comprised 4 litters
258 and Cohort 3 comprised 5 litters (a replicate Cohort of Cohort 2) were tested during a critical time
259 window (PND 21-23) for hyperthermia-induced seizures. Finally, to further investigate *KCNT1*'s
260 potential influence on respiratory physiology, Cohort 4 mice comprised of littermates from 8 litters
261 that underwent whole body plethysmography (WBP). Given that age-matched males are larger
262 than females in body weight and size, both contributing parameters that influence the volume of

263 air respirated during the plethysmograph diagnosis, Cohort 4 subjects were sex-separated to
264 eliminate sex-originating variables for WBP presentation and analysis.

265 ***(i) Open Field Locomotion*** Exploratory locomotion in a novel open field environment was assayed
266 in a room illuminated at ~40lux in a 40 cm×40 cm×30.5 cm arena as previously described[28-31].
267 Exploratory locomotion is an essential assay for gross motor abilities and physical activity over
268 time, identifying key motoric phenotypes, that utilize a conserved neural circuit from flies to
269 humans.

270 ***(ii) Rotarod*** Motor coordination, balance, and motor learning were assessed using an Ugo-Basile
271 accelerating rotarod (Stoelting Co, Wood Dale, IL) as previously published[32-34]. Mice are placed
272 on a rotating cylinder that slowly increases from 4 to 40 revolutions per min (rpm) over a 5min
273 trial, with 3 trials per day using a 60min inter-trial interval, and subsequently repeated over 3
274 consecutive days for a total of 9 trials. Performance was scored as latency to fall (sec) from the
275 cylinder with a maximum latency of 300sec.

276 ***(iii) Whole Body Plethysmography (WBP)*** Whole-body plethysmography (WBP) chambers
277 (Buxco, Data Sciences International, St. Paul, MN) were utilized to assess respiratory parameters,
278 such as inhalation/exhalation volumes, as well as the occurrence and time spent in apneas (an
279 absence of inhaling or exhaling).

280 ***(iv) Electroconvulsive Seizure Threshold (ECT)*** Low intensity (5mA with a 0.9 ms pulse width,
281 299 Hz, for 200 msec), electroconvulsive shock was administered via ear clamps to assess seizure
282 threshold via an ECT Racine Scale consisting of: (0) walks away, (1) brief stun and walks away,
283 (2) very brief jaw, forelimb clonus, lasting less than 1sec, (3) prolonged jaw, forelimb clonus,
284 ventral or dorsal neck flexion, loss of posture, lasting several secs, (4) tonic extension of forelimbs
285 (90 degree angle to torso), (5) tonic extension of hind limbs (90 degree angle to torso). The ECT

286 Racine Scale is unique in that animals typically experience a single seizure event resulting in a
287 single score and then recover over time.

288 ***(v) Seizure susceptibility by a Lethal Dose of the Chemoconvulsant Pentylenetetrazol (PTZ)***
289 Dosing was conducted between 9am-2pm in a well-lit room and followed our validated dosing
290 regimens for C57BL/6J. Subjects were weighed and administered PTZ (70 mg/kg, i.p.), then
291 placed in a clean, empty cage with subsequent seizure stages live scored using a modified Racine
292 scale for a maximum of 30mins. Stages scored were: (1) first jerk/Straub's tail, (2) loss of righting
293 reflex, (3) generalized clonic-tonic seizure, (4) full tonic extension, (5) death. The PTZ Racine
294 Scale is unique in that animals typically progress through the stages over time beginning with 1
295 and ending at 5.

296 ***(vi) Hyperthermia-induced Seizure Susceptibility*** Postnatal day (PND) 21-23 subjects were
297 utilized to reflect the same approximate vulnerable developmental window as the human
298 population[35,36]. Subjects were habituated in an adjacent room for at least 30mins in low light (~30
299 lux). Subjects were given a brief anesthetic exposure (0.1ml 4% isoflurane for 30sec to 1min until
300 loss of consciousness) for insertion of rectal temperature probe (Physitemp RET-4, Clifton, NJ,
301 USA), prior to placement in the testing arena. A heat lamp placed above the arena was positioned
302 at a distance to maintain an internal body temperature of 37.5°C for a 10min habituation period.
303 Following arena habituation, the distance of the heat lamp was dynamically adjusted to avoid rapid
304 overheating and gradually raise the internal body temperature evenly by approximately 0.5°C
305 every 2mins. Testing continues until a behavioral seizure score of 3 or above is observed or until
306 the body's internal temperature reaches 42.5°C, in which case the heat lamp is immediately turned
307 off and distanced from the arena to allow the subject to cool to 40°C proceeded by removal. An
308 observer blind to genotype records the type of seizure using a modified Racine Scale (1. Staring,

309 2. Head nodding, 3. Unilateral forelimb clonus, 4. Bilateral forelimb clonus, 5. Rearing and falling,
310 6. Clonic seizure) previously described by[37]. The febrile Racine Scale is unique in that animals
311 typically progress through the stages over time and then recover once they are removed from the
312 heat source. Animals are returned to their home cage and provided hydrogel once they are active
313 and exhibit normal ambulatory behavior (~30mins).

314 ***Statistical Analysis*** Data were analyzed with GraphPad Prism by two-tailed Student's t-test for
315 single parameter comparison between the two genotypes or a One-Way Repeated Measures
316 ANOVA for comparison of genotype over time (e.g. development, open field, pre-and post-fear
317 conditioning). Significance levels were set at $p<0.05$. Significant ANOVAs were followed by
318 Bonferroni-Dunn posthoc testing.

319

320 **Results.**

321 ***Mouse model generation.*** The *KCNT1* gene sequences differ slightly between human and mouse:
322 the altered amino acid in the G288S human KCNT1 variant is at amino acid position 269 in the
323 mouse protein (**Fig. 1**). Genome editing with CRISPR/Cas9 was used to make the mouse model:
324 the WT mouse *Kcnt1* exon 11 codon (GGG) was replaced with AGC to create the missense
325 mutation. This leads to glycine (G) being replaced by serine (S) at amino acid position 269
326 (G269S) in the mouse Kcnt1 protein this new allele ($Kcnt1^{em1Bryd}$) was nucleotide sequence
327 verified. The mutation was generated on a C57BL/6J genetic background and was maintained by
328 backcrossing heterozygous animals to B6/J and B6/NJ mice.

329 ***High-Density microelectrode array analysis reveals distinct network activity patterns in***
330 ***$Kcnt1^{+/G269S}$ and $Kcnt1^{G269S/G269S}$.*** To investigate the functional consequences of the *Kcnt1* G269S
331 mutation at the network level, we employed high-density microelectrode array (HD-MEA)
332 recordings of primary cortical neurons from wild-type ($Kcnt1^{+/+}$), heterozygous ($Kcnt1^{+/G269S}$), and
333 homozygous ($Kcnt1^{G269S/G269S}$) mice. The Maxwell Biosystems HD-MEA platform featuring
334 26,400 electrodes with 1,024 simultaneous recording channels enabled detailed spatial and
335 temporal mapping of neuronal network activity patterns (**Fig. 2A**). Extracellular signals were
336 recorded from multiple channels allowing for precise detection of action potentials across the
337 neuronal population (**Fig. 2B, C**) from DIV 13-21, spanning the critical network formation and
338 early maturation phases. To ensure comparable recording conditions across genotypes, we
339 quantified the percentage of active electrodes: all three genotypes showed similar electrode
340 activation rates (approximately 70-75%, **Fig. 2D**), indicating that the G269S mutation did not
341 significantly affect neuronal viability or density during initial plating and attachment. However,
342 despite similar electrode coverage, mean firing rates (DIV13-21) differed significantly between

343 genotypes (**Fig. 2E;** $F_{(2,168)}$=13.21, p<0.0001) in a gene-dosage dependent manner: *Kcnt1*$^{G269S/G269S}$
344 neurons had the highest mean firing rate (4.50±0.28 Hz), followed by *Kcnt1*$^{+/G269S}$ (3.56 ± 0.14Hz)
345 and *Kcnt1*$^{+/+}$ neurons (2.84±0.15 Hz). Tukey's post hoc tests revealed that *Kcnt1*$^{G269S/G269S}$ neurons
346 fired significantly more than *Kcnt1*$^{+/G269S}$ (p=0.001) and *Kcnt1*$^{+/+}$ neurons (p<0.0001); while
347 Kcnt1$^{+/G269S}$ neuronal firing rate did not reach significance from *Kcnt1*$^{+/+}$ (p=0.051).
348 ***Network development and bursting dynamics.*** Early network development corresponds to DIV
349 13 when synchronous activity begins to emerge and spread across the neuronal population[38,39],
350 while DIV 27 represents the mature network phase characterized by established bursting patterns
351 and stabilized connectivity[40-42]. At DIV 13, we observed distinctive firing patterns across the three
352 genotypes (**Fig. 3A-C** $F_{(2,52)}$=6.515, p=0.003). During this network formation phase,
353 *Kcnt1*$^{G269S/G269S}$ cultures displayed more frequent bursting activity compared to *Kcnt1*$^{+/+}$ (tukey's
354 post hoc p=0.002), with *Kcnt1*$^{+/G269S}$ networks showing intermediate burst frequency
355 (tukey$_{Kcnt1+/+ \text{vs} Kcnt1+/G269S}$ p=0.039; tukey $_{Kcnt1+/G269S \text{vs} Kcnt1G269S/G269S}$ p=0.199). By DIV 27, the
356 differences in activity patterns became more pronounced but showed a different trajectory than at
357 DIV 13 (**Fig. 3D-F** $F_{(2,40)}$=14.60, p<0.0001). While *Kcnt1*$^{+/+}$ and *Kcnt1*$^{+/G269S}$ cultures maintained
358 consistent bursting patterns with increased synchronization characteristic of mature networks,
359 *Kcnt1*$^{G269S/G269S}$ cultures exhibited markedly diminished burst amplitude and altered burst patterns
360 (tukey$_{Kcnt1+/+ \text{vs} Kcnt1G269S/G269S}$ p=0.149; tukey$_{Kcnt1+/G269S \text{vs} Kcnt1G269S/G269S}$ p<0.0001). This unexpected
361 reversal in the homozygous phenotype suggests potential network dysfunction emerging with
362 prolonged exposure to hyperexcitability, possibly through excitotoxic mechanisms.
363 ***Temporal evolution of network hyperexcitability.*** Quantitative analysis of burst frequency across
364 developmental timepoints (**Fig. 3G** $F_{TIME(2,109)}$=7.516, p=0.0003; $F_{GENOTYPE(2,52)}$=8.027, p=0.0009)
365 revealed a striking biphasic pattern in *Kcnt1*$^{G269S/G269S}$ cultures. Between DIV 13-17,

366 *Kcnt1*$^{G269S/G269S}$ networks exhibited significantly higher burst counts (107.9± 7.21) per recording,
367 compared to *Kcnt1*$^{+/+}$ (62.00 ± 7.41, tukey's p=0.002) reflecting initial hyperexcitability during
368 network formation. However, bursting activity declined in *Kcnt1*$^{G269S/G269S}$ networks (87.19± 7.31)
369 with frequency falling below *Kcnt1*$^{+/+}$ levels (108.4± 5.34) by DIV 24-27 ($F_{(2,40)}$=9.77, p=0.0004;
370 tukey's p=0.162). In contrast, *Kcnt1*$^{+/G269S}$ cultures increased burst frequency over development,
371 showing significantly elevated activity (95.15±4.74; tukey's p=0.0003) at DIV13-17 compared to
372 *Kcnt1*$^{+/+}$ and rising to *Kcnt1*$^{+/+}$ levels (129.40±6.91 tukey's p=0.121) by DIV 24-27. Meanwhile,
373 *Kcnt1*$^{+/G269S}$ cultures burst frequency was below *Kcnt1*$^{G269S/G269S}$ networks at DIV 13-17 (tukey's
374 p=0.275) and rose above their levels by DIV 24-27 (tukey's p=0.0002). This indicates that the
375 *Kcnt1*$^{+/G269S}$ confers a persistent and sustainable hyperexcitability phenotype that remains
376 compatible with ongoing network function, unlike *Kcnt1*$^{G269S/G269S}$.

377 Further analysis of the firing pattern variability was performed, using the Fano factor, the
378 variance-to-mean ratio of spike counts, where a higher Fano factor reflects the healthy stochastic
379 variability essential for proper circuit formation and refinement[43]. *Kcnt1*$^{+/+}$ networks maintained
380 high Fano factor values (**Fig. 3H,** 656.31 ± 71.94; DIV 13 $F_{(2,51)}$=7.057, p=0.002; DIV 27
381 $F_{(2,39)}$=12.36, p<0.0001). In contrast, both *Kcnt1*$^{G269S/G269S}$ (303.11 ± 32.09; tukey's p=0.004;) and
382 *Kcnt1*$^{+/G269S}$ networks (326.67 ± 28.08; tukey's p=0.003) showed significantly lower values during
383 early network formation DIV 13. While the Fano factor of *Kcnt1*$^{+/G269S}$ networks gradually
384 increased toward *Kcnt1*$^{+/+}$ levels by DIV 27 (tukey's p=0.253), *Kcnt1*$^{G269S/G269S}$ networks remained
385 locked in an abnormally regularized firing pattern (tukey's p<0.001). This developmental
386 trajectory—initial hyperexcitability followed by progressive reduction in network activity in
387 *Kcnt1*$^{G269S/G269S}$ cultures, contrasted with sustained hyperexcitability in *Kcnt1*$^{+/G269S}$ cultures—
388 suggests that the G269S GOF mutation affects network development in a gene-dosage dependent

389 manner. Based on these electrophysiological findings, we decided to pursue only the *Kcnt1*$^{+/G269S}$

390 model for subsequent *in vivo* behavioral characterization.

391 ***Exploratory locomotion and motor coordination in the G288S Kcnt1*$^{+/G269S}$ *mouse model.*** Novel

392 exploration in the open field was assessed between age, sex matched littermate controls, for effects

393 resulting from *Kcnt1*$^{+/G269S}$. Total activity across a 30min session illustrated an effect over time in

394 both genotypes (**Fig. 4A**; $F_{TIME(3,148)}$=7.706, p<0.0001), showing acclimation to the arena, as

395 expected. A trend toward hyperactivity in the *Kcnt1*$^{+/G269S}$ mice was observed (**Fig. 4A**;

396 $F_{(1,42)}$=0.6074, p=0.4404) when the 30min session was summed (**Fig. 4B**; $t_{(1,40)}$=2.156, p=0.0372).

397 Motor coordination and motor learning were measured using the accelerating rotarod. We

398 observed a significant reduction in latencies to fall in *Kcnt1*$^{+/G269S}$ compared to *Kcnt1*$^{+/+}$ age

399 matched mice (**Fig. 4C**; $F_{GENOTYPE(1,42)}$=6.79, p=0.0126) indicating poor motor coordination.

400 However, over the three training days we observed improved performance over time, (**Fig. 4C**;

401 $F_{TIME(2,84)}$=36.05, p<0.0001), in both genotypes illustrating intact motor learning.

402 ***Cognitive ability assessed by two standardized assays in the Kcnt1*$^{+/G288S}$ *mouse model is intact.***

403 Cognitive ability was assessed in two different tasks novel object recognition (NOR) memory and

404 fear conditioning. During the familiarization phase of the NOR task, Kcnt*1*$^{+/G269S}$ mice explored

405 the objects substantially less than the *Kcnt1*$^{+/+}$ control mice (**Fig. S1A**: $F_{FAMILIARIZATION}$

406 $_{GENOTYPE(1,29)}$=0.00306, p<0.0001), with a mean investigation time in *Kcnt1*$^{+/+}$ subjects of

407 52.285sec, while in *Kcnt1*$^{+/G269S}$ the mean investigation time was 26.865sec. During the novel

408 investigation phase, both genotypes spent greater time investigating the novel object, versus the

409 familiar object (**Fig. S1B**: $F_{Kcnt1+/+\ (1,41)}$=4.813, p<0.05 and $F_{Kcnt1+/G269S(1,36)}$=18.50, p<0.001). The

410 discrimination index was calculated by dividing the difference in investigation time between the

411 novel and familiar object by the total amount of exploration of both objects (**Fig. S1C**:

412 $t_{(1,40)}$=0.7566), clearly illustrating a lack of cognitive impairments in this assay. Cued and
413 contextual fear conditioning illustrated a strong effect of training (learning from the tone-shock
414 pairings (UCS-CS) (**Fig. S1D**; $F_{TRAINING(1,40)}$=107.8, p<0.0001). While a genotype by training
415 interaction was observed, (**Fig. S1D**; $F_{TRAININGvsGENOTYPE(1,40)}$=4.951, p<0.04), no genotype effect,
416 during training, was observed, (**Fig. S1D**; $F_{GENOTYPE(1, 40)}$=0.7672, p=0.3863), which is a key
417 control metric, since no genotype effect across training allows for the investigation of differences
418 in memory and recall. Contextual recall 24 hrs. after UCS-CS training did not differ between
419 genotypes (**Fig. S1E**; $t_{(1,50)}$=0.4610, p=0.6468). However, cued recall, performed 48hrs after initial
420 training, illustrated recall of the cued-shock pairing by high levels of freezing illustrated post cue
421 but not pre cue in *Kcnt1*$^{+/G269S}$ compared to *Kcnt1*$^{+/+}$ age matched mice (**Fig. S1F**; $F_{CUE(1,40)}$=11.05,
422 p<0.0001).

423 ***Behavioral seizure quantification, in the Kcnt1$^{+/G269S}$ mouse model by multiple methods.*** Firstly,
424 susceptibility to seizures early in life (post-natal day 21-23) was induced by hyperthermia,
425 analogous to fever induced (febrile) seizures in Cohort 2 animals. Susceptibility was measured by
426 probability to develop behavioral seizures, temperature to first seizure, and severity of seizure by
427 a modified Febrile Racine score. *Kcnt1*$^{+/G269S}$ animals had a higher average Febrile Racine score
428 than *Kcnt1*$^{+/+}$ controls (**Fig. 5A**: $t_{(1,31)}$=2.146, p<0.05) and a lower temperature threshold (**Fig. 5B**:
429 $t_{(1,16)}$=2.849, df=16, p<0.01). *Kcnt1*$^{+/G269S}$ animals also had an increased probability of developing
430 a behavioral seizure (**Fig. 5C**: χ2=7.506, p<0.0005), over their *Kcnt1*$^{+/+}$ counterparts. Importantly,
431 a replicate Cohort by a separate investigator produced similar results (**Fig. S2A-C**). Following
432 behavioral assay completion, Cohort 1 mice were measured for epileptic progression after
433 induction with electro- and chemoconvulsant seizures. Seizures in Cohort 1 animals were first
434 induced by ear-clip electroconvulsive threshold (ECT) wherein animals reached similar seizure

435 levels (**Fig. 5D**: $t_{(1, 40)}$=0.17, p=0.86) and recovered post-seizure induction in less than 5 minutes
436 (**Fig. 5E**: $t_{(1,37)}$=1.28, p=2.08). Both *Kcnt1*$^{+/G269S}$ and *Kcnt1*$^{+/+}$ animals had similar probability of
437 recovery post-seizure experience (**Fig. 5F**: χ2=7.506, p=0.65). Following PTZ administration at
438 70 mg/kg, a lethal dose, *Kcnt1*$^{+/G269S}$ and *Kcnt1*$^{+/+}$ mice reached each seizure stage at similar rates
439 (**Fig. 5G**: $F_{(1,37)}$=0.01, p=0.92), including latency to first jerk, latency to loss of righting, latency
440 to generalized clonic-tonic seizure, latency to full extension, and latency to death. Additionally,
441 the probability of survival was similar between *Kcnt1*$^{+/G269S}$ and *Kcnt1*$^{+/+}$ animals (**Fig. 3H**:
442 $F_{(1,12)}$=0.499, p=0.49). Taken together, the *Kcnt1*$^{+/G269S}$ animals were highly sensitive to early life
443 heat-induced seizures, as opposed to the adult exposure to either electroconvulsive or
444 chemoconvulsive induced seizures. Since the ECT and PTZ seizure inductions were conducted in
445 the same animals we correlated the seizure severity between the two induction methods, in order
446 to determine if one would be predictive of the other, i.e., correlation (**Fig. S3**). Latency to first jerk
447 after PTZ administration was negatively correlated with seizure severity in ECT in *Kcnt1*$^{+/+}$
448 animals (**Fig. S3A** r=-0.46, p=0.05). While latency to generalized tonic-clonic PTZ seizures were
449 negatively correlated with seizure severity after ECT in *Kcnt1*$^{+/G269S}$ (**Fig S3G** r=-0.57, p=0.02).
450 Together these correlations indicate that mice that experienced the most intense responses to ECT,
451 also moved more quickly through the Racine scale stages during PTZ induced seizures.

452 ***Respiratory parameters identified erratic breathing and apnea in the Kcnt1$^{+/G288S}$ mouse model.***
453 Our laboratory was interested in defining respiratory metrics at baseline, given KCNT1-related
454 epilepsy's increased incidence of Sudden Unexpected Death in Epilepsy (SUDEP) and elevated
455 apneas[44-46]. Animals were assessed for 2hrs during the light cycle for respiratory parameters in the
456 whole-body plethysmography (WBP) chambers. *Kcnt1*$^{+/G269S}$ and *Kcnt1*$^{+/+}$ breathing
457 characteristics were quantified, including indices such as inspiration and expiration volumes, as

458 well as the presence of apneas. Animals were separated by sex as aged matched female mice are
459 smaller than their male counterparts resulting in inherent sex differences for these measures.
460 Percentage of time spent breathing normal was similar between *Kcnt1*$^{+/G269S}$ and *Kcnt1*$^{+/+}$ females
461 (**Fig. 6A**: $t_{(1,18)}$=0.4896, p=0.6297), whereas males exhibited decreased normal breathing
462 ($t_{(1,17)}$=2.391, p=0.0258). Additionally, males and females of both genotypes had similar levels of
463 erratic breathing (**Fig. 6B**: females $t_{(1,18)}$=1.675, p=0.1094; males $t_{(1,17)}$=0.7847, p=0.4410). Lastly,
464 the number of apnea events was elevated in *Kcnt1*$^{+/G269}$ mice in males (**Fig. 6C**: $t_{(1,17)}$,t=2.391,
465 p=0.0258) and not in females ($t_{(1,18)}$,t=0.4896, p=0.6297), compared to their respective sex matched
466 *Kcnt1*$^{+/+}$ controls. Taken together, this data may indicate that male *Kcnt1*$^{+/G269S}$ mice experience
467 more respiratory difficulties than age matched females.
468

469 **Discussion.**

470 Herein, we generated a novel experimental model for *KCNT1*-related epilepsy and
471 channelopathies, a subgroup of neurodevelopmental disorders. This model mouse carries the
472 mouse equivalent (G269S) of the human GOF variant G288S. CRISPR/Cas9 was used in
473 C57BL/6J mice to replace the WT gene codon GGG with AGC, creating the missense mutation
474 that substitutes glycine (G) to serine (S) at amino acid position 269 in the mouse Kcnt1 protein.
475 The new allele (*Kcnt1*^{em1Bryd}) was nucleotide sequence verified, and the mice were maintained on
476 C57BL6/NJ and were donated to the Mutant Mouse Resource and Research Center
477 (MMRRC:075727-MU). Although the initial model was maintained on a C57BL/6NJ background,
478 we backcrossed it onto C57BL/6J to align with existing models of developmental and epileptic
479 encephalopathy (DEE) and rare genetic neurodevelopmental disorders (NDDs). However, we
480 acknowledge the limitations of the C57BL/6J strain in seizure studies, as documented in prior
481 literature[18-20,47-49]. Given the reported differences in seizure susceptibility and responsiveness
482 between sub strains, future experiments may return to the C57BL/6NJ background to better
483 understand how genetic background influences phenotype, particularly of spontaneous recurrent
484 seizures (SRS), seizure induction and potential of therapeutic testing[18,50]. Such comparisons are
485 essential for evaluating the generalizability of findings and optimizing translational relevance[51].

486 We performed functional characterization of primary cortical neurons from *Kcnt1*$^{+/+}$,
487 *Kcnt1*$^{+/G269S}$, and *Kcnt1*$^{G269S/G269S}$ mice *in vitro* revealing gene dose-dependent differences in
488 excitability. Homozygous *Kcnt1*$^{G269S/G269S}$ cultures showed an initial phase of hyperexcitability
489 followed by network collapse, while heterozygous *Kcnt1*$^{+/G269S}$ cultures maintained sustained
490 hyperexcitability. Strikingly, both mutant genotypes exhibited a ~50% reduction in firing pattern
491 variability (Fano factor: *Kcnt1*$^{+/+}$ ≈ 656 vs. mutants ≈ 300–327), indicating abnormally regularized

492 activity. This loss of stochastic variability likely disrupts normal circuit development [43]. These
493 findings are consistent with known cell type-specific effects of KCNT1 gain-of-function (GOF)
494 variants, which disproportionately impair inhibitory neurons—particularly non-fast-spiking
495 GABAergic interneurons[13,52]. The G269S mutation, located in the channel pore region, appears
496 especially severe: homozygous cultures lost bursting activity by DIV 28, suggesting excitotoxicity
497 due to excessive firing. In contrast, the heterozygous model retains viable hyperexcitability, more
498 accurately reflecting the human condition and offering a robust platform for therapeutic
499 development. These findings suggest that approaches targeting improved inhibitory tone and
500 excitation-inhibition balance, rather than KCNT1 channel blockade alone, may prove more
501 effective for treating *KCNT1*-related epilepsies[53-55].

502 Next, we discovered that *Kcnt1*$^{+/G269S}$ mice exhibited seizures following early life
503 hyperthermia, a preclinical assay utilized as an analog for febrile seizures or seizures resulting
504 from high temperature fevers[37]. Compared to age-matched control littermates, *Kcnt1*$^{+/G269S}$ mice
505 experienced seizure onset at lower temperatures, had a higher incidence of seizures, and scored
506 higher on a modified febrile Racine scale, indicating increased severity across two Cohorts. In
507 contrast, adult *Kcnt1*$^{+/G269S}$ mice that were subjected to a 2-hit seizure paradigm—induction by
508 electroconvulsive threshold (ECT) followed by a high dose of pentylenetetrazol (PTZ, 70
509 mg/kg)—were indistinguishable from *Kcnt1*$^{+/+}$ controls, on every metric. Finally, a tailored
510 behavioral phenotyping battery was performed on a seizure naïve Cohort of *Kcnt1*$^{+/G269S}$ and
511 *Kcnt1*$^{+/+}$ littermates that included: developmental milestones, exploratory locomotion, motor
512 coordination and motor learning, novel object learning and memory, and contextual and cued
513 learning and memory. Additionally, we evaluated respiratory physiology using whole-body
514 plethysmography (WBP), which was included given the clinical reports of asthma and pulmonary

515 hemorrhage in *KCNT1*-related epilepsy[56-59], as well as the presence of apneas leading to disrupted
516 sleep as a common occurrence in genetic NDDs, particularly when facial dysmorphic traits are
517 evident[60-62]. While *Kcnt1*$^{+/G269S}$ and *Kcnt1*$^{+/+}$ littermates were developmentally indistinguishable,
518 *Kcnt1*$^{+/G269S}$ mice were hyperactive in the 30min open field arena and lacked motor coordination
519 on days 1 and 2 on the rotarod. Finally, *Kcnt1*$^{+/G269S}$ mice exhibited increased apneas and erratic
520 breathing which align with the clinical presentation.

521 In summary, we report for the first time a novel Kcnt1 G269S knock-in mouse model,
522 backcrossed onto the C57BL/6J background. This model represents a significant advancement in
523 the study of *KCNT1*-related epilepsy, developmental and epileptic encephalopathies (DEEs), and
524 neurodevelopmental channelopathies. We hypothesize that early-life seizures, as observed in this
525 model, are driving phenotypes that closely align with clinical features of *KCNT1*-related epilepsy,
526 including motor hyperactivity, learning and memory impairments, apneas, spontaneous seizures,
527 and sleep disturbances. Notably, homozygous *Kcnt1*$^{G269S/G269S}$ mice are not construct valid, thus
528 reducing the relevance, required for translational research, and making this heterozygous model
529 ideal for both *in vitro* and *in vivo* therapeutic testing.

530 Limited clinical success of KCNT1 channel blockers such as quinidine has been well
531 documented[53,54,63-65]. This work illustrates that future therapeutic strategies may be more effective
532 if they focus on: (i) restoring inhibitory tone; (ii) reducing potassium efflux; and (iii) correcting
533 excitation-inhibition (E/I) imbalance. Future studies will incorporate long-term wireless EEG to
534 assess cortical activity, including spiking, spike trains, sleep architecture, and spectral power
535 density over multiple days. Cortical EEG is a critical translational biomarker and is routinely used
536 by our lab and others[26,37,66-68], especially given the nuance of the C57BL6/J background strain[69].
537 Moreover, we will report sensory evoked potentials, another common translational biomarker.

538 Additionally, our adult ECT experiments were conducted using ear-clip stimulation at low
539 intensity. Based on recommendations from the Frankel lab (personal communication), we have
540 since modified our ECT apparatus to allow for transcorneal stimulation at higher intensities. This
541 implementation will be reported in future studies, as data is currently being acquired. These
542 analyses have the ability to illustrate the severity of this GOF variant and enable deeper *in vivo*
543 phenotyping. These enhancements will contribute to a more comprehensive understanding of
544 *KCNT1* variant effects and support improved patient stratification.

545 The G288S mutation was originally identified via whole-exome sequencing in two
546 unrelated patients with early-onset DEE[65]. As previously noted, this variant does not correspond
547 to a single epilepsy subtype[70], highlighting the importance of understanding how G288S/G269S
548 modulates network excitability, insights will inform therapeutic development, and might yield
549 information relevant to the most affected individuals and inform stratification. Groundwork in
550 *KCNT1*-related epilepsy was outlined by many as summarized in **Table 1**, but we must highlight
551 generous contributions and personal communication with the Wayne Frankel laboratory
552 (Columbia University) who generated the first ever mouse models, the knock-in (KI), human
553 variants Y777H and Y796H and illustrated motor cortex hyperexcitability, early-onset seizures,
554 and hyperactivity in KI/KI mice[16,52]. In 2024, Wu et al. discovered the R455H mutation which
555 exhibited increased sodium conductance, increased excitatory neuron activity, and suppression of
556 excitability in inhibitory interneurons in a mouse model, which altered sodium channel expression,
557 with effect sizes of 4-6-fold increases in KI/KI mice. While previous findings in homozygous
558 variant mice are significant, with substantial effect sizes to test for therapeutic reversal, there
559 remains an unmet need for a more construct valid single copy KI variant model, since affected
560 individuals with *KCNT1*-related epilepsy are heterozygous. The model presented herein has filled

561 this unmet need by its generation and clear phenotypic excitability in cortical neurons and early
562 life heat seizure sensitivity as an *in vivo* outcome measure, malleable for future therapeutic testing,
563 making it a powerful tool for translation and platforms of future therapeutic discovery.

564 **Conclusions**

565 Overall, characterization of *Kcnt1*$^{+/G269S}$ mice indicates a sensitivity to hyperthermia-induced
566 seizures and a motor learning delay. Future studies are required to investigate the impact of early
567 life seizures on adult motor, cognitive, and sleep measures as well as EEG before developing novel
568 therapeutic interventions for individuals with *KCNT1*-related epilepsy.

569

Figure 1. Generation of the *Kcnt1*^{G269S} mutant mouse model.

A) The KCNT1 protein consists of six hydrophobic transmembrane segments with a pore loop domain between the last two transmembrane segments. It also has a large intracellular carboxy-terminal region containing tandem RCK domains and an NAD+ binding domain. The mouse G269S (corresponding to human G288S) mutation, indicated by a red star, occurs within the channel pore. **B)** The mouse model was engineered using CRISPR-Cas9 genome editing to replace the endogenous GGG (Gly) with AGC (Ser). **C)** Confirmation of the engineered DNA base pair changes using Sanger sequencing. The heterozygous sample in the chromatogram shows overlapping G (black) and A (green) peaks for the G to A change and overlapping G (black) and C (blue) peaks for the G to C change.

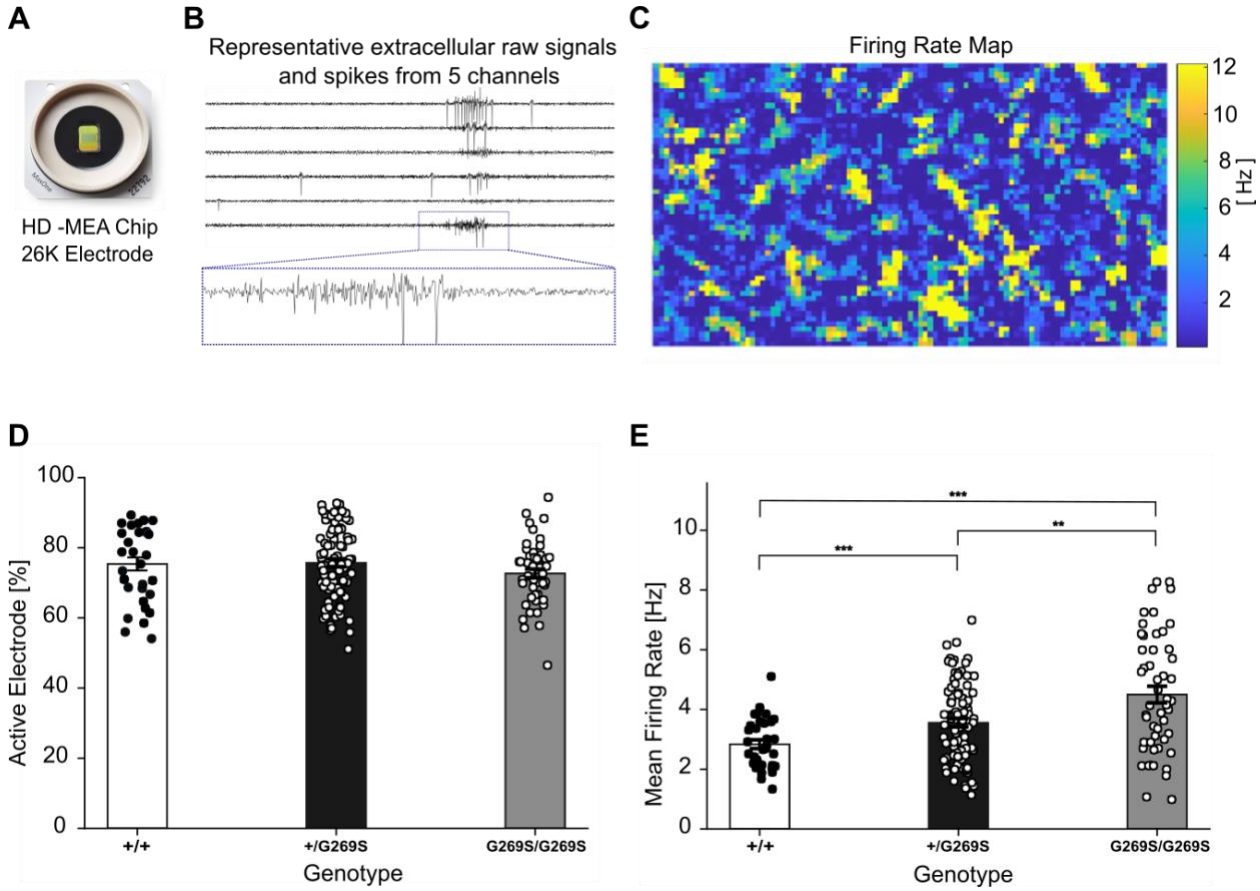

Fig. 2. High-density MEA recordings reveal genotype-dependent differences in neuronal network activity.

(A) Image of the high-density microelectrode array (HD-MEA) chip used in this study (26,000 electrodes; MaxOne platform, Maxwell Biosystems). (B) Example of raw extracellular action potential (eAP) traces recorded from active electrodes. (C) Representative firing rate map from a cortical culture, showing spatial distribution of neuronal activity across the MEA surface. Warmer colors indicate higher firing rates (color scale: 2–12 Hz). (D) Percentage of active electrodes per well for wild-type *Kcnt1*$^{+/+}$, heterozygous *Kcnt1*$^{+/G269S}$, and homozygous *Kcnt1*$^{G269S/G269S,}$ neuronal networks. (E) Quantification of mean firing rate (Hz) across genotypes. *Kcnt1*$^{G269S/G269S}$ neurons fired significantly more than both *Kcnt1*$^{+/G269S}$ ($t = -3.00$, $p = 0.0036$, **) and *Kcnt1*$^{+/+}$($t = 5.27$, $p < 0.0001$, ***), while *Kcnt1*$^{+/G269S}$ neurons also differed significantly from *Kcnt1*$^{+/+}$ ($t = 3.51$, $p = 0.0007$, ***). Bars represent mean ± SEM; individual points reflect biological replicates.

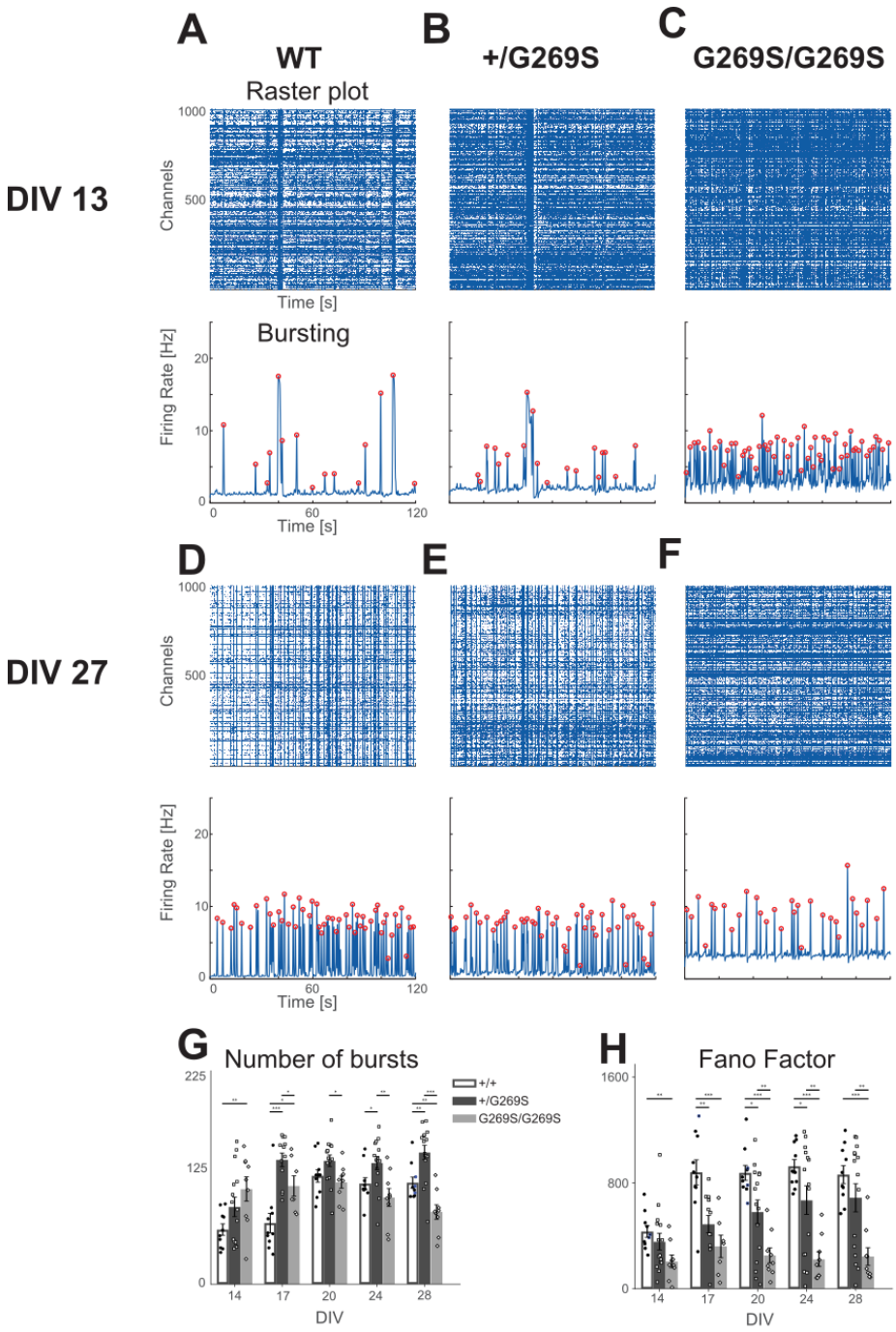

596
597 **Fig. 3. Developmental progression of burst dynamics in *Kcnt1*$^{+/+}$, *Kcnt1*$^{+/G269S}$, and**
598 ***Kcnt1*$^{G269S/G269S}$ in primary neuron culture.**
599 (A–F) Representative raster plots (top) and population firing rate traces (bottom) from wild-type
600 (*Kcnt1*$^{+/+}$, A, D), heterozygous (*Kcnt1*$^{+/G269S}$, B, E), and homozygous (*Kcnt1*$^{G269S/G269S}$, C,F)
601 cortical networks recorded at DIV13 (A–C) and DIV27 (D–F). Each raster shows 120secs of
602 activity across 1024 electrodes. Firing rate traces display synchronized burst events detected using
603 a Gaussian kernel convolution; red dots indicate burst peaks. *Kcnt1*$^{+/+}$ and *Kcnt1*$^{+/G269S}$ networks
604 display sparse, periodic bursts at DIV13 that become more frequent and structured by DIV27. In

605 contrast, *Kcnt1*$^{G269S/G269S}$ networks show highly frequent and irregular bursting at DIV13, followed
606 by diminished activity and synchrony at DIV27. (G) Quantification of burst count across
607 developmental timepoints (DIV13–27). *Kcnt1*$^{G269S/G269S}$ networks display a biphasic pattern with
608 early hyperexcitability (DIV13–17) and later hypoactivity, whereas *Kcnt1*$^{+/G269S}$ cultures maintain
609 and increase burst frequency over the developmental time. (H) Fano factor, a measure of firing
610 variability, is significantly reduced in both mutant genotypes compared to *Kcnt1*$^{+/+}$ at all
611 timepoints, indicating abnormally regularized activity. Bars represent mean ± SEM; individual
612 data points represent biological replicates. Error bars indicate mean +/- SEM. $p < 0.05$ (*), $p <$
613 0.01 (**), $p < 0.001$ (***).
614

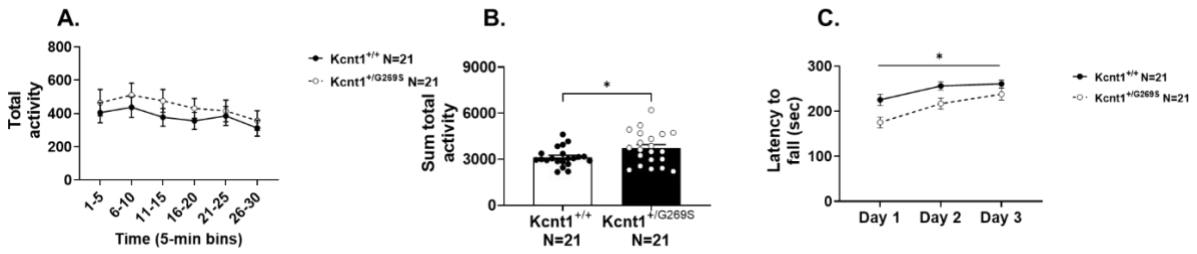

615
616 **Fig. 4. Elevated motor activity in a novel open field arena using the total activity parameter**
617 **over a 30min period in *Kcnt1*$^{+/G269S}$** vs ***Kcnt1*$^{+/+}$.** Gross motor abilities were assessed using
618 activity in a novel open field arena by: A, B) total activity across a 30min session. In Panel A, data
619 are shown in 5min bins. C) *Kcnt1*$^{+/G269S}$ have poor motor coordination compared to *Kcnt1*$^{+/+}$
620 controls using the standard accelerating rotarod paradigm. Error bars indicate mean +/- SEM. *
621 $p<0.05$
622

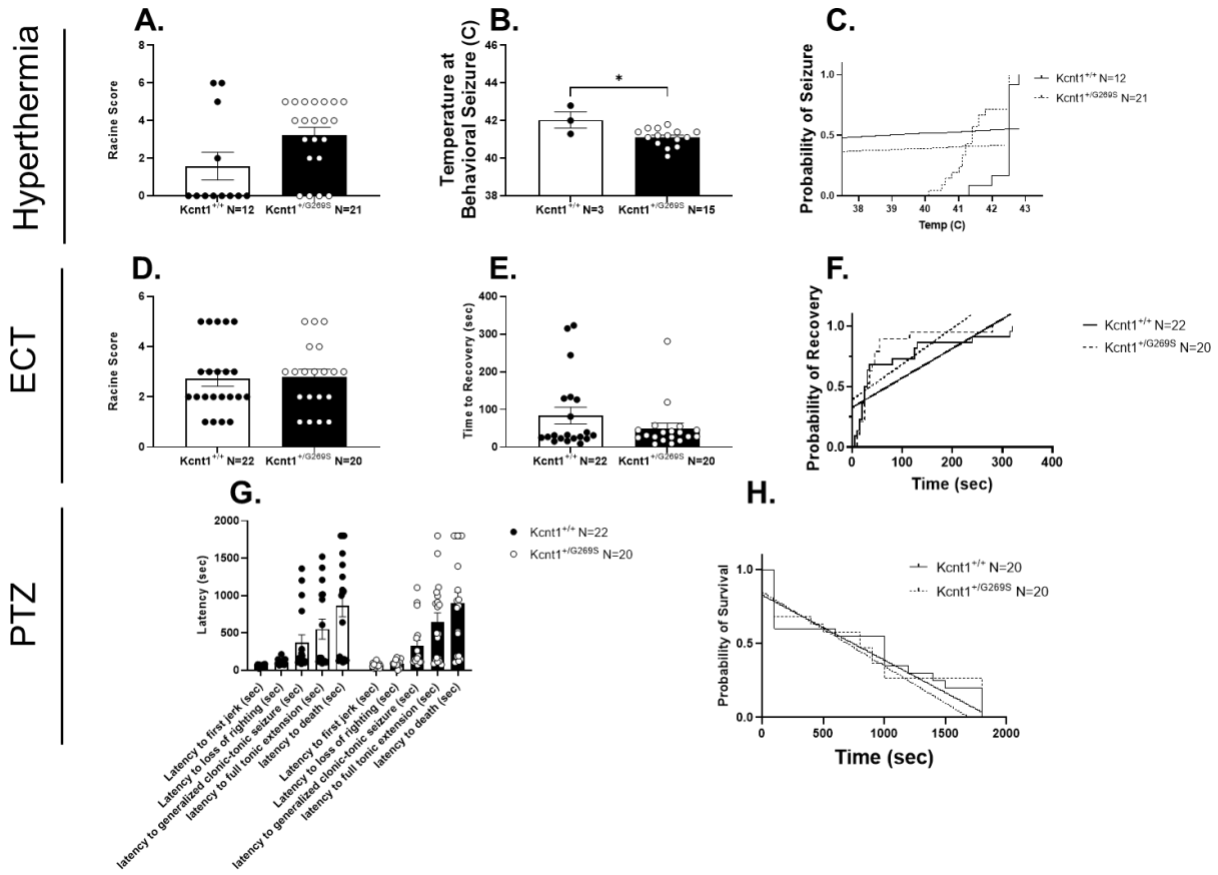

Figure 5: Seizure responsiveness to Hyperthermia-, Electroconvulsive-, and Chemoconvulsive-induction.

A) Seizure severity using modified Febrile Racine scale to Hyperthermia-induced seizure. B) Average temperature to behavioral seizure. C) Probability of behavioral seizure as temperature is increased. D) Seizure severity using a modified ECT Racine scale in response to electroconvulsive shock threshold (ECT; 5mA with a 0.9ms pulse width, 299 Hz, for 200 msec). E) Time to recovery (sec) post ECT induction. F) Probability of recovery post ECT. G) Latency to each stage of a modified Racine scale in response to chemoconvulsive treatment with pentylenetetrazole (PTZ, i.p., 70 mg/kg). H) Probability of survival post PTZ. Error bars indicate mean +/- SEM. * $p<0.05$.

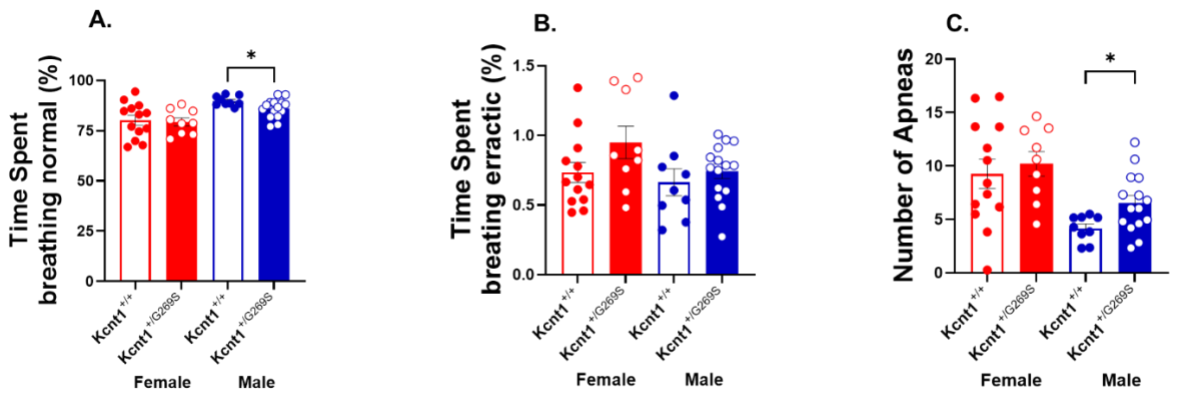

634

635 **Fig. 6: Respiratory apneas and erratic breathing assessed by whole body plethysmography**
636 **(WBP) in *Kcnt1*$^{+/G269S}$ and *Kcnt1* $^{+/+}$ mice.** Whole body plethysmography evaluation for A) % of
637 time breathing normal, B) % of Time breathing erratic, C) number of apneas. Error bars indicate
638 mean +/- SEM. * $p<0.05$

639

640 **References**
641

642 1 Satterstrom, F. K. *et al.* Large-Scale Exome Sequencing Study Implicates Both Developmental
643 and Functional Changes in the Neurobiology of Autism. *Cell* **180**, 568-584 e523 (2020).
644 https://doi.org/10.1016/j.cell.2019.12.036
645 2 Noebels, J. Precision physiology and rescue of brain ion channel disorders. *J Gen Physiol* **149**,
646 533-546 (2017). https://doi.org/10.1085/jgp.201711759
647 3 Daghsni, M. *et al.* Autism throughout genetics: Perusal of the implication of ion channels. *Brain*
648 *Behav* **8**, e00978 (2018). https://doi.org/10.1002/brb3.978
649 4 Sanders, S. J. *et al.* Progress in Understanding and Treating SCN2A-Mediated Disorders. *Trends*
650 *Neurosci* **41**, 442-456 (2018). https://doi.org/10.1016/j.tins.2018.03.011
651 5 Smith, R. S. & Walsh, C. A. Ion Channel Functions in Early Brain Development. *Trends Neurosci*
652 **43**, 103-114 (2020). https://doi.org/10.1016/j.tins.2019.12.004
653 6 Niemi, M. E. K. *et al.* Common genetic variants contribute to risk of rare severe
654 neurodevelopmental disorders. *Nature* **562**, 268-271 (2018). https://doi.org/10.1038/s41586-
655 018-0566-4
656 7 Almog, Y. *et al.* Developmental alterations in firing properties of hippocampal CA1 inhibitory and
657 excitatory neurons in a mouse model of Dravet syndrome. *Neurobiol Dis* **148**, 105209 (2021).
658 https://doi.org/10.1016/j.nbd.2020.105209
659 8 Hinckley, C. A. *et al.* Functional evaluation of epilepsy-associated KCNT1 variants in multiple
660 cellular systems reveals a predominant gain of function impact on channel properties. *Epilepsia*
661 **64**, 2126-2136 (2023). https://doi.org/10.1111/epi.17648
662 9 Bonardi, C. M. *et al.* KCNT1-related epilepsies and epileptic encephalopathies: phenotypic and
663 mutational spectrum. *Brain* **144**, 3635-3650 (2021). https://doi.org/10.1093/brain/awab219
664 10 Rychkov, G. Y. *et al.* Functional Effects of Epilepsy Associated KCNT1 Mutations Suggest
665 Pathogenesis via Aberrant Inhibitory Neuronal Activity. *Int J Mol Sci* **23** (2022).
666 https://doi.org/10.3390/ijms232315133
667 11 Quraishi, I. H. *et al.* An Epilepsy-Associated KCNT1 Mutation Enhances Excitability of Human
668 iPSC-Derived Neurons by Increasing Slack K(Na) Currents. *J Neurosci* **39**, 7438-7449 (2019).
669 https://doi.org/10.1523/JNEUROSCI.1628-18.2019
670 12 Lim, C. X., Ricos, M. G., Dibbens, L. M. & Heron, S. E. KCNT1 mutations in seizure disorders: the
671 phenotypic spectrum and functional effects. *J Med Genet* **53**, 217-225 (2016).
672 https://doi.org/10.1136/jmedgenet-2015-103508
673 13 Wu, J., Quraishi, I. H., Zhang, Y., Bromwich, M. & Kaczmarek, L. K. Disease-causing Slack
674 potassium channel mutations produce opposite effects on excitability of excitatory and
675 inhibitory neurons. *Cell Rep* **43**, 113904 (2024). https://doi.org/10.1016/j.celrep.2024.113904
676 14 Burbano, L. E. *et al.* Antisense oligonucleotide therapy for KCNT1 encephalopathy. *JCI Insight* **7**
677 (2022). https://doi.org/10.1172/jci.insight.146090
678 15 Wang, R., Teng, S., Turanchik, M., Zhen, F. & Peng, Y. Tonic-clonic seizures induce hypersomnia
679 and suppress rapid eye movement sleep in mouse models of epilepsy. *Sleep Adv* **6**, zpaf009
680 (2025). https://doi.org/10.1093/sleepadvances/zpaf009
681 16 Shore, A. N. *et al.* Heterozygous expression of a Kcnt1 gain-of-function variant has differential
682 effects on SST- and PV-expressing cortical GABAergic neurons. *bioRxiv* (2024).
683 https://doi.org/10.1101/2023.10.11.561953
684 17 Vanderver, A. *et al.* Identification of a novel de novo p.Phe932Ile KCNT1 mutation in a patient
685 with leukoencephalopathy and severe epilepsy. *Pediatr Neurol* **50**, 112-114 (2014).
686 https://doi.org/10.1016/j.pediatrneurol.2013.06.024

687 18 Copping, N. A., Adhikari, A., Petkova, S. P. & Silverman, J. L. Genetic backgrounds have unique
688 seizure response profiles and behavioral outcomes following convulsant administration. *Epilepsy*
689 *Behav* **101**, 106547 (2019). https://doi.org/10.1016/j.yebeh.2019.106547
690 19 Miller, A. R., Hawkins, N. A., McCollom, C. E. & Kearney, J. A. Mapping genetic modifiers of
691 survival in a mouse model of Dravet syndrome. *Genes Brain Behav* **13**, 163-172 (2014).
692 https://doi.org/10.1111/gbb.12099
693 20 Yang, Y. & Frankel, W. N. Genetic approaches to studying mouse models of human seizure
694 disorders. *Adv Exp Med Biol* **548**, 1-11 (2004). https://doi.org/10.1007/978-1-4757-6376-8_1
695 21 Zhang, Q., Liu, Y., Xu, J., Teng, Y. & Zhang, Z. The Functional Properties, Physiological Roles,
696 Channelopathy and Pharmacological Characteristics of the Slack (KCNT1) Channel. *Adv Exp Med*
697 *Biol* **1349**, 387-400 (2021). https://doi.org/10.1007/978-981-16-4254-8_18
698 22 Ehaideb, S. *et al.* Allostatic Compensatory Mechanisms Enable the Mutant KCNT1 Channels to
699 Induce Seizures and Hyperexcitability. *iScience* (2018). https://doi.org/
700 http://dx.doi.org/10.2139/ssrn.3188397
701 23 Seiler, S. *et al.* Astrocyte-derived factors regulate CNS myelination. *Glia* **72**, 2038-2060 (2024).
702 https://doi.org/10.1002/glia.24596
703 24 Hanes, A. L. *et al.* Divergent Synaptic Scaling of Miniature EPSCs following Activity Blockade in
704 Dissociated Neuronal Cultures. *J Neurosci* **40**, 4090-4102 (2020).
705 https://doi.org/10.1523/JNEUROSCI.1393-19.2020
706 25 Ben-Shalom, R., Aviv, A., Razon, B. & Korngreen, A. Optimizing ion channel models using a
707 parallel genetic algorithm on graphical processors. *J Neurosci Methods* **206**, 183-194 (2012).
708 https://doi.org/10.1016/j.jneumeth.2012.02.024
709 26 Fenton, T. A. *et al.* Hyperexcitability and translational phenotypes in a preclinical mouse model
710 of SYNGAP1-related intellectual disability. *Transl Psychiatry* **14**, 405 (2024).
711 https://doi.org/10.1038/s41398-024-03077-6
712 27 Sharma, S., Puttachary, S., Thippeswamy, A., Kanthasamy, A. G. & Thippeswamy, T. Status
713 Epilepticus: Behavioral and Electroencephalography Seizure Correlates in Kainate Experimental
714 Models. *Front Neurol* **9**, 7 (2018). https://doi.org/10.3389/fneur.2018.00007
715 28 Adhikari, A. *et al.* Touchscreen cognitive deficits, hyperexcitability and hyperactivity in males and
716 females using two models of Cdkl5 deficiency. *Hum Mol Genet* **31**, 3032-3050 (2022).
717 https://doi.org/10.1093/hmg/ddac091
718 29 Copping, N. A. *et al.* Neuronal overexpression of Ube3a isoform 2 causes behavioral
719 impairments and neuroanatomical pathology relevant to 15q11.2-q13.3 duplication syndrome.
720 *Hum Mol Genet* **26**, 3995-4010 (2017). https://doi.org/10.1093/hmg/ddx289
721 30 Gompers, A. L. *et al.* Germline Chd8 haploinsufficiency alters brain development in mouse. *Nat*
722 *Neurosci* **20**, 1062-1073 (2017). https://doi.org/10.1038/nn.4592
723 31 Silverman, J. L., Babineau, B. A., Oliver, C. F., Karras, M. N. & Crawley, J. N. Influence of
724 stimulant-induced hyperactivity on social approach in the BTBR mouse model of autism.
725 *Neuropharmacology* **68**, 210-222 (2013). https://doi.org/10.1016/j.neuropharm.2012.07.042
726 32 Berg, E. L. *et al.* Insulin-like growth factor-2 does not improve behavioral deficits in mouse and
727 rat models of Angelman Syndrome. *Mol Autism* **12**, 59 (2021). https://doi.org/10.1186/s13229-
728 021-00467-1
729 33 Huie, E. Z. *et al.* Peptidomimetic inhibitors targeting TrkB/PSD-95 signaling improves cognition
730 and seizure outcomes in an Angelman Syndrome mouse model. *Neuropsychopharmacology* **50**,
731 772-782 (2025). https://doi.org/10.1038/s41386-024-02020-z
732 34 Petkova, S. P. *et al.* Gait as a quantitative translational outcome measure in Angelman
733 syndrome. *Autism Res* **15**, 821-833 (2022). https://doi.org/10.1002/aur.2697

35 Symonds, J. D. *et al.* Incidence and phenotypes of childhood-onset genetic epilepsies: a prospective population-based national Cohort. *Brain* **142**, 2303-2318 (2019). https://doi.org/10.1093/brain/awz195

36 Cottam, N. C. *et al.* From Circuits to Lifespan: Translating Mouse and Human Timelines with Neuroimaging-Based Tractography. *J Neurosci* **45** (2025). https://doi.org/10.1523/JNEUROSCI.1429-24.2025

37 Born, H. A. *et al.* Early Developmental EEG and Seizure Phenotypes in a Full Gene Deletion of Ubiquitin Protein Ligase E3A Rat Model of Angelman Syndrome. *eNeuro* **8** (2021). https://doi.org/10.1523/ENEURO.0345-20.2020

38 Bikbaev, A., Frischknecht, R. & Heine, M. Brain extracellular matrix retains connectivity in neuronal networks. *Sci Rep* **5**, 14527 (2015). https://doi.org/10.1038/srep14527

39 Cabrera-Garcia, D. *et al.* Early prediction of developing spontaneous activity in cultured neuronal networks. *Sci Rep* **11**, 20407 (2021). https://doi.org/10.1038/s41598-021-99538-9

40 Vertes, P. E., Alexander-Bloch, A. & Bullmore, E. T. Generative models of rich clubs in Hebbian neuronal networks and large-scale human brain networks. *Philos Trans R Soc Lond B Biol Sci* **369** (2014). https://doi.org/10.1098/rstb.2013.0531

41 Spencer, M. C. *et al.* Multiscale evolving complex network model of functional connectivity in neuronal cultures. *IEEE Trans Biomed Eng* **59**, 30-34 (2012). https://doi.org/10.1109/TBME.2011.2171340

42 Downes, J. H. *et al.* Emergence of a small-world functional network in cultured neurons. *PLoS Comput Biol* **8**, e1002522 (2012). https://doi.org/10.1371/journal.pcbi.1002522

43 Wagenaar, D. A., Pine, J. & Potter, S. M. Searching for plasticity in dissociated cortical cultures on multi-electrode arrays. *J Negat Results Biomed* **5**, 16 (2006). https://doi.org/10.1186/1477-5751-5-16

44 Moller, R. S. *et al.* Mutations in KCNT1 cause a spectrum of focal epilepsies. *Epilepsia* **56**, e114-120 (2015). https://doi.org/10.1111/epi.13071

45 Kuchenbuch, M. *et al.* KCNT1 epilepsy with migrating focal seizures shows a temporal sequence with poor outcome, high mortality and SUDEP. *Brain* **142**, 2996-3008 (2019). https://doi.org/10.1093/brain/awz240

46 Chorny, L. E., Nordli, D. R., 3rd & Galan, F. Breath-holding spells: A typical case with EEG and video correlate. *Epileptic Disord* (2024). https://doi.org/10.1002/epd2.20324

47 Frankel, W. N., Taylor, L., Beyer, B., Tempel, B. L. & White, H. S. Electroconvulsive thresholds of inbred mouse strains. *Genomics* **74**, 306-312 (2001). https://doi.org/10.1006/geno.2001.6564

48 Mistry, A. M. *et al.* Strain- and age-dependent hippocampal neuron sodium currents correlate with epilepsy severity in Dravet syndrome mice. *Neurobiol Dis* **65**, 1-11 (2014). https://doi.org/10.1016/j.nbd.2014.01.006

49 Sukoff Rizzo, S. J., McTighe, S. & McKinzie, D. L. Genetic Background and Sex: Impact on Generalizability of Research Findings in Pharmacology Studies. *Handb Exp Pharmacol* **257**, 147-162 (2020). https://doi.org/10.1007/164_2019_282

50 Calsbeek, J. J. *et al.* Persistent neuropathology and behavioral deficits in a mouse model of status epilepticus induced by acute intoxication with diisopropylfluorophosphate. *Neurotoxicology* **87**, 106-119 (2021). https://doi.org/10.1016/j.neuro.2021.09.001

51 Sittig, L. J. *et al.* Genetic Background Limits Generalizability of Genotype-Phenotype Relationships. *Neuron* **91**, 1253-1259 (2016). https://doi.org/10.1016/j.neuron.2016.08.013

52 Shore, A. N. *et al.* Reduced GABAergic Neuron Excitability, Altered Synaptic Connectivity, and Seizures in a KCNT1 Gain-of-Function Mouse Model of Childhood Epilepsy. *Cell Rep* **33**, 108303 (2020). https://doi.org/10.1016/j.celrep.2020.108303

53 Numis, A. L. *et al.* Lack of response to quinidine in KCNT1-related neonatal epilepsy. *Epilepsia* **59**, 1889-1898 (2018). https://doi.org/10.1111/epi.14551

54 Xu, D. *et al.* Precision therapy with quinidine of KCNT1-related epileptic disorders: A systematic review. *Br J Clin Pharmacol* **88**, 5096-5112 (2022). https://doi.org/10.1111/bcp.15479

55 Liu, C. Q. *et al.* Efficient strategies based on behavioral and electrophysiological methods for epilepsy-related gene screening in the Drosophila model. *Front Mol Neurosci* **16**, 1121877 (2023). https://doi.org/10.3389/fnmol.2023.1121877

56 Cassibba, J. *et al.* Pulmonary Hemorrhage Revealing Multiple Vascular Malformations in a Child with KCNT1 Developmental Epileptic Encephalopathy. *J Pediatr* **237**, 311-312 (2021). https://doi.org/10.1016/j.jpeds.2021.06.019

57 Chauhan, D., Verhoeven, P. A., Kohli, U., Udassi, J. P. & Mascio, C. E. Life-threatening pulmonary haemorrhage treated with coil embolisation followed by lobectomy in a patient with KCNT1 mutation. *Cardiol Young* **34**, 701-703 (2024). https://doi.org/10.1017/S104795112300447X

58 Garancini, N. *et al.* Pulmonary vascular malformations in genetic epileptic encephalopathy: A rare, fatal case report. *Respir Med Case Rep* **53**, 102155 (2025). https://doi.org/10.1016/j.rmcr.2024.102155

59 Kawasaki, Y. *et al.* Three Cases of KCNT1 Mutations: Malignant Migrating Partial Seizures in Infancy with Massive Systemic to Pulmonary Collateral Arteries. *J Pediatr* **191**, 270-274 (2017). https://doi.org/10.1016/j.jpeds.2017.08.057

60 Fusco, A. F. *et al.* Respiratory dysfunction in a mouse model of spinocerebellar ataxia type 7. *Dis Model Mech* **14** (2021). https://doi.org/10.1242/dmm.048893

61 Gertler, T., Bearden, D., Bhattacharjee, A. & Carvill, G. in *GeneReviews((R))* (eds M. P. Adam *et al.*) (1993).

62 Hagebeuk, E. E., van den Bossche, R. A. & de Weerd, A. W. Respiratory and sleep disorders in female children with atypical Rett syndrome caused by mutations in the CDKL5 gene. *Dev Med Child Neurol* **55**, 480-484 (2013). https://doi.org/10.1111/j.1469-8749.2012.04432.x

63 Jia, Y. *et al.* Quinidine Therapy for Lennox-Gastaut Syndrome With KCNT1 Mutation. A Case Report and Literature Review. *Front Neurol* **10**, 64 (2019). https://doi.org/10.3389/fneur.2019.00064

64 Lin, Z. *et al.* Efficacy of Anti-seizure Medications, Quinidine, and Ketogenic Diet Therapy for KCNT1-Related Epilepsy and Genotype-Efficacy Correlation Analysis. *Front Neurol* **12**, 834971 (2021). https://doi.org/10.3389/fneur.2021.834971

65 Rizzo, F. *et al.* Characterization of two de novoKCNT1 mutations in children with malignant migrating partial seizures in infancy. *Mol Cell Neurosci* **72**, 54-63 (2016). https://doi.org/10.1016/j.mcn.2016.01.004

66 Copping, N. A. & Silverman, J. L. Abnormal electrophysiological phenotypes and sleep deficits in a mouse model of Angelman Syndrome. *Mol Autism* **12**, 9 (2021). https://doi.org/10.1186/s13229-021-00416-y

67 Gonzalez, E. A. *et al.* Sex-specific acute and chronic neurotoxicity of acute diisopropylfluorophosphate (DFP)-intoxication in juvenile Sprague-Dawley rats. *Curr Res Toxicol* **2**, 341-356 (2021). https://doi.org/10.1016/j.crtox.2021.09.002

68 Haigh, J. L. *et al.* Deletion of a non-canonical regulatory sequence causes loss of Scn1a expression and epileptic phenotypes in mice. *Genome Med* **13**, 69 (2021). https://doi.org/10.1186/s13073-021-00884-0

69 Purtell, H. *et al.* Electrographic spikes are common in wildtype mice. *Epilepsy Behav* **89**, 94-98 (2018). https://doi.org/10.1016/j.yebeh.2018.09.003

70 Andreone, B. J. *et al.* Durable suppression of seizures in a preclinical model of KCNT1 genetic epilepsy with divalent small interfering RNA. *Epilepsia* (2025). https://doi.org/10.1111/epi.18278

Translational Stage	Subjects/Model System	Genotypes Tested	Phenotypes found	
Clinical	5 female and 7 male MMPSI patients	A934T; R428Q; R474H; I760M	EEG: migrating seizures. Brain MRI: delayed myelination, thin corpus callosum. Hypotonia	
Clinical	248 patients	152 EIMFS; 37 DEE; 53 ADNFLE and 6 with other phenotypes	Literature review: clinical seizures, sleep disturbances, hypotonia, and other features	
Clinical	43 patients	n=1 unless otherwise stated: A477T; A934T; R398Q; R398Leu; R428Q (n=2); R474H (n=3); R929Q; R950Q (n=3); R961H; R961S; Q651R; G288S (n=3); K947E; F932S	Quinidine treatment resulted in a >50% seizure reduction in patients with G288S; F932S; R961S; R950Q; A477T while seizures worsened for 3 patients with R474H variant.	
Clinical	30 patients: 17 boys and 13 girls	not specified	Ketogenic diet therapy was effective regardless of the variant, especially effective in patients with functional domain variant-related epilepsy. Quinidine was effective in patients with non-functional domain variant-related epilepsy.	
Preclinical (human sequence)	Human iPSC-derived neurons	Homozygous P924L	Sodium-dependent potassium currents are increased; duration of action potentials is decreased in current clamp recordings with an increase in the total number of action potentials	
Preclinical (human DNA sequence; non neuronal specific)	HEK293T cells	T314A	decreased current amplitude abolished channel activation	
		G288S, R398Q, N449S, L781V, E893K, M896V, F932L, R928C, S937G, L942F, R961H, A965T	increased current amplitude	
		L781V, E893K, M896V, R928C, F932L	increased channel open probabilities	
Preclinical (human DNA sequence; non neuronal specific)	*Xenopus laevis* oocytes and HEK cell lines	36 variants	significant increases in current magnitude for G288S, A934T, R389Q, R428Q, and R474H variants. G288S and R398Q increased channel kinetics. R474H reduced channel kinetics. 28 of 33 variants tested had GOF impacts on current magnitude, V1/2, or both	

Preclinical (species specific DNA sequence; non neuronal specific)	*Xenopus laevis* oocyte	hKCNT1 mutations M896I, R398Q, Y796H, R928C, R428Q, A934T, P924L and the rat rKcnt1 mutant R907C	KCNT1 mutations increase current magnitude and hasten (M896I, R928C and A934T) or slow (R398Q) activation, increase current amplitude, and modulate channel kinetics. Quinidine at 300uM was effective in blocking current amplitude with varying sensitivity.	
In vivo preclinical	*Drosophila*	hKCNT1, G288S, R928C	Increases in K+ conductance, hyper excitability and seizures	Eha
In vivo and *In vitro* preclinical	*Drosophila* and HEK293T cells	hKCNT1, G288S, R398Q or R928C	Expression in GABAergic neurons resulted in seizure phenotypes resistant to carbamazepine, valproic acid, vigabatrin, quinidine, and cannabidiol.	
In vivo and *In vitro* preclinical	CHO cells and mice	Cells: L456F of human KNa1.1 Mouse: Kcnt1 L457F Background strain: C57BL/6J	No significant differences between genotypes on Rotarod, Zero maze, Open Field, home cage. No differences by GT to seizure susceptibility by flurothyl (20ul/min). While KI/+ and KI/KI mice were susceptible to both Kainate (30mg/kg) and Pentylenetrazole (60mg/kg) induction.	
In vitro preclinical (neuronal specific)	Mouse primary neurons	Y796H (mouse Y777H) Background strain: C57BL/6NJ	No effects on glutamatergic or VIP neuron function. SST neurons became hypoexcitable with a higher rheobase current and lower action potential firing frequency, whereas PV neurons became hyperexcitable with a lower rheobase current and higher AP firing frequency	
In vivo preclinical	Mice	Y796H (mouse Y777H) Background strain: C57BL/6NJ	Alterations in GABAergic neurons including hyperexcitability and hyper-synchronicity. Additional Epileptiform activity was found in HOM mice only via Video-EEG.	

In vivo preclinical	Mice	Y796H (mouse Y777H) crossed with Snap25-GCaMP6s Background strain: C57BL/6NJ	Widefield Ca2+ imaging in HOM and WT mice showed no differences in mesoscale interictal activity	T
In vivo preclinical	Mice and *Xenopus laevis* oocytes	Y796H (mouse Y777H) Background strain: C57BL/6 13 hKCNT1B variants	hKCNT1B and variants were characterized in *Xenopus laevis* oocytes for activity and responsiveness to 13 potassium channel blockers, of which tipepidine and hydroquinine were the most effective. Additionally, these two drugs were effective at blocking spontaneous seizures in Y777H HOM mice.	
In vivo preclinical	Mice	Y796H (mouse Y777H) generated on background strain C57BL/6NJ, but backcrossed to C57BL/6J in this study (number of crossings not specified)	Spontaneous seizures in KCNT1 HOM mice occur during NREM sleep and suppress REM sleep. (NREM: synchronized EEG with high-amplitude, delta frequency [0.5–4 Hz] activity and low EMG activity; REM: high power at theta frequencies [6–9 Hz] and low EMG activity)	
In vivo preclinical	Mice	R474H (mouse R455H) developed on C57BL/6J and backcrossed for 4-5 generations Knock-out mice (Kcnt1$^{-/-}$) developed on Sv/129 and backcrossed with C57BL/6NJ for 2 generations. WTs were from a parallel colony of Sv/129 backcrossed with C57BL/6NJ	Knock out mice were hypoactive in open field and on the rotarod, with no differences in seizure susceptibility from WT. Homozygous R455H was embryonic lethal. R455H/+ mice had increased spontaneous seizures in EEG and a decreased threshold for PTZ (60mg/kg) induced seizures compared to WT with no motor differences in the open field or rotarod	
In vitro and *Ex Vivo* preclinical	Mouse primary neurons and slice	R474H (mouse R455H) Background strain: C57BL/6J	Na+-dependent K+ (KNa) and voltage-dependent sodium (NaV) currents are increased in both excitatory and inhibitory cortical neurons leading to increases in firing of excitatory neurons and suppressing firing of inhibitory neurons.	

In vivo preclinical	Mice	Knock-out mice (Kcnt1$^{-/-}$) developed on C57BL/6J and backcrossed to C57BL/6NJ for >6 generations	Complete loss of hippocampal LTP and LTD, Reduced NMDA receptor signaling, suppresses the expression of multiple proteins that localize to axons, dendrites and myelin sheath, but increases levels of inner mitochondrial membrane proteins	
		R455H/+ Background strain: C57BL/6J	Some protein changes, but much milder compared to KO. ASO treatment did reverse some of the protein changes seen in this model	

832 **Table 1. Summary of clinical and preclinical data using model systems or clinical studies**
833 **related to the novel translational model herein, *Kcnt1*$^{+/G288S}$.**

834